ACS OMEGA

Open Access

http://pubs.acs.org/journal/acsodf

Article

Mechanism of V-Shaped Pits on Promoting Hole Injection in the InGaN MQWs: First-Principles Investigation

Qingqing Feng, Li Liu, Yu Zhang, Xiaolu Zhu, Hai Kuang, Mingbin Zhou, Juanli Zhao, Ning Wu, and Zhihua Xiong*

Cite This: *ACS Omega* 2024, 9, 7163−7172

Read Online

ACCESS | Metrics & More | Article Recommendations

ABSTRACT: In the InGaN multiple quantum wells (MQWs), V-shaped pits play a crucial role in carrier transport, which directly affects emitting efficiency. First-principles calculations are applied to investigate the formation of the V-shaped pits, and the results indicate that they are inclined to form in the N-rich environment. Meanwhile, we calculate the interfacial electronic properties of the sidewalls of the V-shaped pits with varying indium (In) and magnesium (Mg) compositions. The calculated valence band offset (VBO) of the $In_{0.3}Ga_{0.7}N/Ga_{0.94}Mg_{0.06}N$ (0001) is 0.498 eV, while that of the $In_{0.07}Ga_{0.93}N/Ga_{0.94}Mg_{0.06}N$ ($10\bar{1}1$) is 0.340 eV. The band alignment results show that the valence band edges in the $Ga_{1-y}Mg_yN$ layer are in higher energy than in the $In_xGa_{1-x}N$ layer. These are in good agreement with the values reported in the previous numerical simulation. Moreover, the calculation of the projected density of states (PDOS) of interfaces discloses that the strong hybridization between the N 2p orbital and the Mg 2p orbital exerts a vital influence on the upward shifts of the valence band edges in the superlattices (SLs). All these results reveal that holes are easier to inject into the quantum wells (QWs) via the sidewall of V-shaped pits rather than the *c*-plane QWs, providing a theoretical basis for the growth of InGaN MQWs samples containing V-shaped pits.

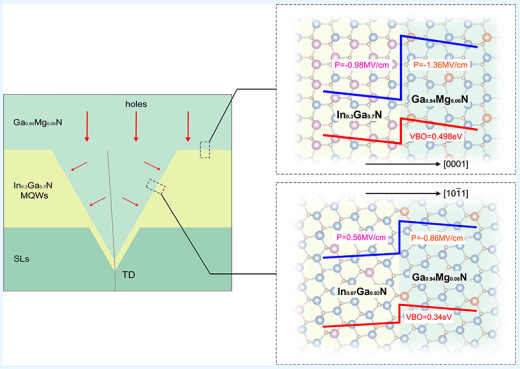

1. INTRODUCTION

The III−V nitride semiconductor GaN and its alloy InGaN, owing to their excellent performance, have exhibited brilliant performance in the fields of lighting, displays, and other areas.[1−4] However, a high density of threading dislocations (TDs) will be generated during the epitaxy process of multiple quantum wells (MQWs) because of the poor matching in the lattice parameter and the thermal expansion coefficient between the epi-layer and foreign substrate.[5,6] As reported by many literature studies, V-shaped pit defects with six {$10\bar{1}1$}-oriented sidewalls are generated from TDs.[7−12]

As for the effect that V-shaped pits have on the emission efficiency of the MQWs, tremendous efforts have been exerted, and there are some controversial views. Some researchers hold that the V-shaped pits along with the TDs behave as nonradiative recombination (NR) centers and provide a leakage current pathway; thus, it is essential to suppress the growth of the V-shaped pits.[13−17] On the other hand, as reported by many researchers, the V-shaped pits have positive effects on increasing the internal quantum efficiency (IQE). For example, Hangleiter et al. put forward that the V-shaped pits can suppress NR around TDs. The narrower sidewall quantum wells (QWs) of V-shaped pits (for convenience, called sidewall QWs in the following) and the lower indium (In) composition of sidewall QWs provide an effective band barrier which can prevent the carriers from NR.[18] Subsequently, researchers realized the positive effect of the V-shaped pits and used this theory to explain why low-dislocation-density AlGaInP light-emitting diodes (LEDs) have low luminous efficiency, while high-dislocation-density InGaN LEDs exhibit high luminous efficiency.[19]

A number of researchers subsequently confirmed this screening effect of the V-shaped pits through experimental measurements[20−23] and some studies found that the sample with V-shaped pits exhibited higher output power than the one without.[5,24] Moreover, to improve IQE, many studies are devoted to getting an optimized size of V-shaped pits by changing superlattice (SL) periods[25−27] and SL growth temperature.[27,28] For example, Chang et al.[25] explored the effect of V-shaped pit size on the IQE of the InGaN/GaN MQWs by varying the number of SL periods. They concluded

Received: November 19, 2023
Revised: December 27, 2023
Accepted: January 5, 2024
Published: January 29, 2024

that the optimal size of a V-shaped pit is approximately 200−250 nm for MQWs with 15 SL periods. Meanwhile, there are also literature studies dedicated to researching the screening efficiency of V-shaped pits of different sizes.[21,22] Kim et al. conducted monochromatic cathodoluminescence (CL) research and observed that the dark region in small V-shaped pits is about eight times as large as their physical sizes while it is about the same in the large pits.[22] The regional brightness represents the higher intensity of radiative recombination in the CL research;[29,30] thus, they held that the energy barrier provided by different sizes of V-shaped pits is different. Cho et al. found that the NR can be suppressed effectively when the energy barrier height is larger than about 80 meV.[21] These researches indicate that V-shaped pits can significantly improve IQE, and several groups[5,31−34] have conducted plenty of thorough studies on the mechanism.

By growing InGaN/GaN blue MQWs and measuring the electroluminescence spectra, Li et al. investigated the effect that the V-shaped pits have on hole injection.[31] They found that the large V-shaped pits are of great importance for the hole injection depth. By numerical simulation, Quan et al. reported that V-shaped pits can promote hole injection and thus enhance the optical performance of the GaN-based MQWs.[5] In addition, Li et al. employed three-dimensional numerical modeling to study the influence of the V-shaped pits on the current path, which showed that current can flow and be injected into the deeper lateral QWs through the sidewalls of V-shaped pits.[34]

However, there has been no relevant report studying the interfacial physical properties of sidewall QWs. Studying the interfacial electronic properties is of great significance for understanding the mechanism of V-shaped pits in promoting hole injection and providing theoretical guidance in the experimental growth manipulation of V-shaped pits experimentally.

In this work, first-principles calculations are performed to investigate the formation of V-shaped pits; meanwhile, the physical properties of their sidewall QWs are studied to explore the mechanism of V-shaped pits in promoting hole injection. First, we calculate the formation energy of three sizes of V-shaped pits and the band alignment of $Ga_{1-y}Mg_yN$ and the sidewall QWs (the top QW) interfaces. Then, to further understand the band alignment results, we perform projected density of states (PDOS) and polarization electric field calculation. In the end, we discuss the effect of V-shaped pits on hole injection by constructing an energy-band diagram (Figure 1).

2. MODELS AND CALCULATION METHODS

2.1. Models. A supercell of 6 × 6 × 5 GaN (0001) surface slab that contains 396 atoms is constructed by using the plane slab method. To discuss the formation mechanism of V-shaped pits in InGaN MQWs, three sizes of V-shaped pits that are defined as V1 (slab model with one Ga vacancy), V3 (slab model with four Ga vacancies and one N vacancy), V5 (slab model with 11 Ga vacancies and four N vacancies), respectively, are established, as displayed in Figure 2. Meanwhile, all these V-shaped pits are N-terminated.[35−38] A vacuum region of 13 Å is set in these GaN (0001) surface slab models, and the pseudohydrogen atoms with 0.75 e^- are used to passivate the bottom N dangling bonds. Additionally, the pseudohydrogen atoms and bottom two bilayers of GaN are fixed while the rest are enabled to relax during the calculation.

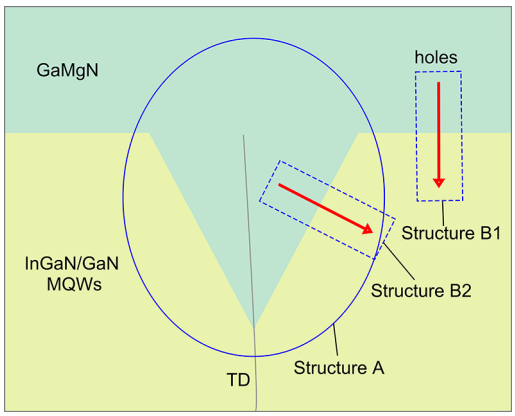

Figure 1. Schematic structure of InGaN/GaN MQWs with a V-shaped pit embedded. It is worth noting that the pit is filled by the GaMgN layer. The red arrows represent the flat injection and sidewall injection of holes.

To further investigate the interfacial properties of the sidewall QWs and the $Ga_{1-y}Mg_yN$ layer, the $In_xGa_{1-x}N/Ga_{1-y}Mg_yN(10\bar{1}1)$ superlattices (SLs) are established on a 288-atom 2 × 2 × 18 wurtzite supercell. Here, we consider the In compositions of $0 \le x \le 0.3$ for $In_xGa_{1-x}N$ in the $(10\bar{1}1)$ SLs and two magnesium (Mg) doping concentrations for $Ga_{1-y}Mg_yN$, i.e., $Ga_{0.94}Mg_{0.06}N$ and $Ga_{0.9}Mg_{0.1}N$. To compare with the above semipolar SLs, we also calculate the interfaces between the top layer in the *c*-plane QWs and the $Ga_{1-y}Mg_yN$, i.e., $GaN/Ga_{1-y}Mg_yN$ (0001) and $In_{0.3}Ga_{0.7}N/Ga_{1-y}Mg_yN$ (0001) interface, as shown in Figure 3a.

2.2. Density Functional Calculations. In this work, first-principles calculations based on density functional theory (DFT) are performed to explore the formation mechanism of V-shaped pits and the interfacial electrical properties of SLs. The Vienna ab initio simulation package (VASP)[39] with the Perdew−Burke−Ernzerhof (PBE) of generalized gradient approximation[40] is used. The energy cutoff is set to 450 and 650 eV for defect and interfacial calculations, respectively. A 2 × 2 × 1 Monkhorst−Pack mesh is used in the first Brillouin zone[41] for both calculations. The 3*d* electrons of Ga and In are regarded as valence electrons. The convergence standard of all of the structural optimizations is 0.05 eV/Å on relaxed atoms for the Hellmann−Feynman forces. For the energy convergence criteria, we set 1×10^{-3} and 1×10^{-4} eV for the calculation of slab and SLs models, respectively. Besides, to calculate the band alignment naturally, the in-plane lattice constants are set to fix, and the out-of-plane lattice constants relax during the atomic relaxation.

2.3. Methodology of Defect Calculation. The formation energy of a defect[42,43] can be written as

$$\Delta H_f = E_{tot}(\text{defect}) - E_{tot}(\text{host}) + n_{Ga}\mu_{Ga} + n_N\mu_N \quad (1)$$

where E_{tot}(host) is the total energy of the surface slab model without defect and E_{tot}(defect) is the total energy of the same surface slab model with a defect. $n = (n_{Ga}, n_N)$ represents the number difference of Ga/N atoms between the defect model and the perfect model. When under extremely Ga-rich conditions, the Ga chemical potential μ_{Ga} reaches its maximum, $\mu_{Ga} = \mu_{Ga[bulk]}$. In the same way, the maximum value of the N chemical potential is $\mu_{N[N_2]}$. For GaN to be thermodynamically stable, μ_N is restricted to the following expression

https://doi.org/10.1021/acsomega.3c09221
ACS Omega 2024, 9, 7163−7172

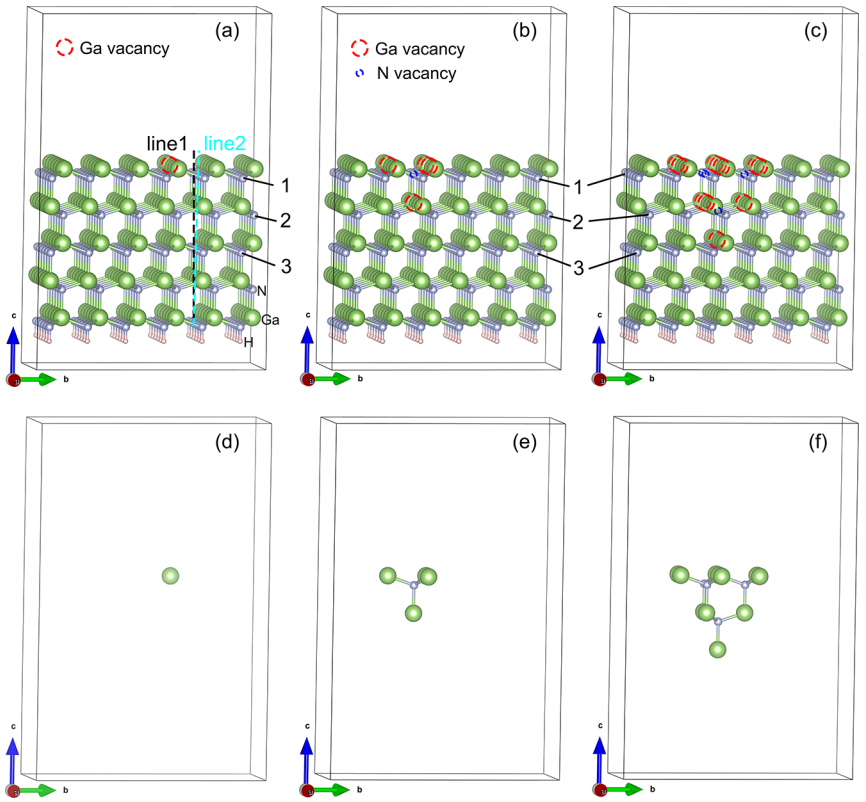

Figure 2. Atomic configurations of Structure A in Figure 1. Calculated slab models of (a) V1, (b) V3, and (c) V5 of V-shaped pits. (d–f) Configurations that are formed by the vacancies in (a–c). The numbers 1–3 in (a–c) represent the three N atomic layers from top to bottom. Line 1 (2) in (a) is connected by the two atomic coordinates along the c direction (the bottom fixed N atom and the relaxed N atom in the 1/2/3 layer before (after) atomic relaxation).

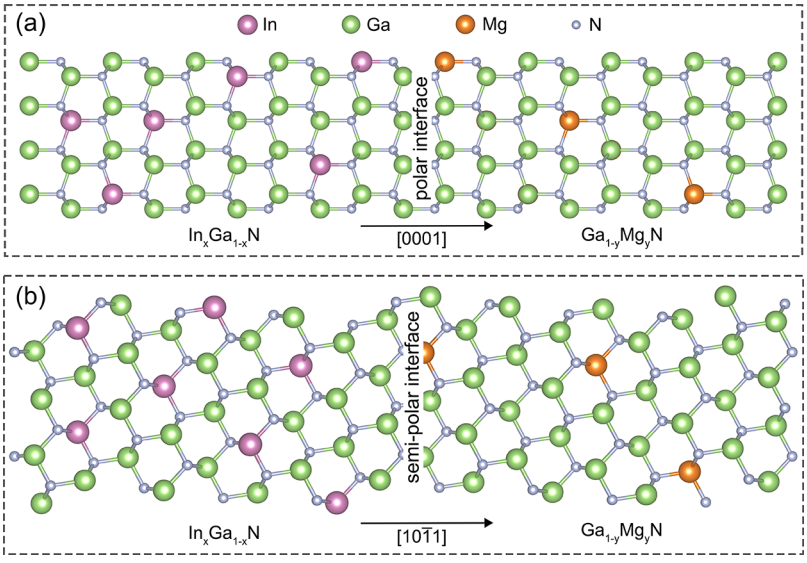

Figure 3. Interface atomic structures of (a) Structure B1 in Figure 1, the polar SL $In_xGa_{1-x}N/Ga_{1-y}Mg_yN$ (0001) and (b) Structure B2 in Figure 1, the semipolar SL $In_xGa_{1-x}N/Ga_{1-y}Mg_yN$ (10$\bar{1}$1).

$$\mu_{Ga} + \mu_N = E_{tot}[GaN] \quad (2)$$

where $E_{tot}[GaN]$ is the total energy of the bulk GaN. According to the above formula, the minimum of μ_{Ga} is determined. Moreover, the total energy of GaN is given by

$$E_{tot}[GaN] = \mu_{Ga[bulk]} + \mu_{N[N_2]} + \Delta H_f[GaN] \quad (3)$$

where $\Delta H_f[GaN]$ is the formation enthalpy. Our calculated $\Delta H_f[GaN]$ is −1.38 eV, being accordance with previous reports.[43−46]

2.4. Methodology of the Band Alignment. The average potential alignment method[47,48] is employed to calculate the band alignment of interfaces. The valence band offset (VBO) is expressed as

https://doi.org/10.1021/acsomega.3c09221
ACS Omega 2024, 9, 7163−7172

$$\mathrm{VBO} = (E_{\mathrm{V}}^{\mathrm{B}} - E_{\mathrm{V}}^{\mathrm{A}}) + \Delta V \quad (4)$$

and the conduction band offset (CBO) is given by

$$\mathrm{CBO} = \Delta E_{\mathrm{g}} - \mathrm{VBO} \quad (5)$$

Here, $E_{\mathrm{V}}^{\mathrm{A}}(E_{\mathrm{V}}^{\mathrm{B}})$ represents the difference between the valence band maximum (VBM) and the average electrostatic potential of the bulk A(B). ΔV represents the potential alignment from the self-consistent calculation of the interface. ΔE_{g} is the difference in the energy gaps of the two independent bulk materials. Typically, when extracting the averaged electrostatic potential on both sides of the SLs, a bulk-like region far from the interface is chosen.

3. RESULTS AND DISCUSSION

3.1. Formation of the V-Shaped Pits. As listed in Table 1, the formation energies of V-shaped pits of three different sizes are obtained under Ga-rich and N-rich environments. It is found that the pits of all three sizes tend to form in the N-rich environment. It can be explained by that N atoms are more likely to bond with Ga atoms in the Ga-rich environment. In the N-rich environment, the N-terminated facet is more likely to form, providing a great environment for the growth of sidewall QWs. Although there are reports claiming that a low V/III ratio is preferable for V-shaped pits to grow, the V/III ratio in epitaxial growth is always larger than 10 and even reaches the order of thousands.[49−52] This rather high ratio indicates that the environment is still N-rich. Our calculated results are consistent with those of these reports. Thus, we hold that the V-shaped pits are inclined to form in the N-rich environment.

Table 1. Calculated Formation Energies (in eV) of V-Shaped Pits of Three Sizes

	formation energy (eV)	
geometry of the V-shaped pit	Ga-rich	N-rich
V1	−3.9444	−5.3268
V3	0.1382	−4.0090
V5	10.7714	1.0946

Based on structural analysis after atomic relaxation, we find that the semipolar $\{10\bar{1}1\}$ is relatively stable. This is obtained indirectly by measuring the angle between line 1 and line 2 in Figure 2a, and the results are listed in Table 2. The relaxed N atoms in Figure 2a are those closest to the V-shaped pits, and the angle is the average value of 1−3 atomic layers. This result indicates the good stability of the $(10\bar{1}1)$ facet because the maximum difference between before and after atomic relaxation is only 0.5°. This can be well explained why the V-shaped pits exhibit $\{10\bar{1}1\}$ facets instead of other facets in experiment.[7−11] Furthermore, the maximum values of the three structures all appear in the measurement data of the bottom layer, and the farther away from the bottom layer, the smaller the value is. This can be ascribed to the mutual repulsion between the same atoms. Taking the V5 model as an example, in the third layer, the distance between the nearest N atoms around the pit is the smallest, and the resulting repulsive force leads to large changes in the atomic positions. From the third layer to the first layer, the measured value decreases as the repulsive force decreases. Therefore, it can be concluded that the $\{10\bar{1}1\}$-oriented sidewall QWs have good stability.

Table 2. Angle Values (in °) between Line 1 and Line 2 for Each 1−3 Layer (in Figure 2) of Three Sizes of V-Shaped Pits

geometry of the V-shaped pit	1st layer	2nd layer	3rd layer
V1	0.03		
V3	0.04	0.50	
V5	0.03	0.17	0.32

3.2. Interfacial Property. The band alignment calculation is a major and direct way to study carrier transport. The conduction and valence band edges of $In_xGa_{1-x}N/Ga_{1-y}Mg_yN$ (0001) and $In_xGa_{1-x}N/Ga_{1-y}Mg_yN$ $(10\bar{1}1)$ interfaces with varying In and Mg compositions are all plotted in Figure 4. Moreover, these figures present several characteristics: (1) both the value of VBO and CBO are increasing with the increased In and Mg compositions for both polar and semipolar SLs; (2) the VBO in semipolar SLs is smaller than that in polar SLs under the same In and Mg compositions; (3) all VBO values are positive. The first feature can be explained by polarization electric fields and orbital hybridization,[53−56] which will be discussed in detail later. Combining the second and third features, it can be concluded that for both polar and semipolar SLs, there is an energy barrier for holes from the $Ga_{1-y}Mg_yN$ to inject into the QWs. The energy barriers of polar SLs are obviously larger than that of semipolar SLs. Taking $In_{0.07}Ga_{0.93}N/Ga_{0.94}Mg_{0.06}N$ $(10\bar{1}1)$ and $In_{0.3}Ga_{0.7}N/Ga_{0.94}Mg_{0.06}N$ (0001) as examples, the energy barrier height for holes from $Ga_{1-y}Mg_yN$ to inject into the sidewall QWs is 0.340 eV, while that for *c*-plane QWs is 0.498 eV. This is extremely consistent with the simulation results of Quan et al.[5] Therefore, we can conclude that holes from the $Ga_{1-y}Mg_yN$ layer are easier to inject into the sidewall QWs of the V-shaped pits than into the *c*-plane QWs.

To further investigate the underlying reason for the increase in VBO with increasing In and Mg compositions, the layer-projected DOS (LDOS) for $GaN/Ga_{1-y}Mg_yN$ (0001), $GaN/Ga_{1-y}Mg_yN$ $(10\bar{1}1)$, $In_{0.3}Ga_{0.7}N/Ga_{1-y}Mg_yN$ (0001) and $In_{0.07}Ga_{0.93}N/Ga_{1-y}Mg_yN$ $(10\bar{1}1)$ (y = 0.06, 0.1) results are obtained in Figure 5. From these LDOSs, it is found that the polarization electric fields increase with the increasing In and Mg compositions in both polar SLs and semipolar SLs. Meanwhile, the calculated polarization electric field data in Table 3 are in good agreement with the above finding. Moreover, the higher the In composition, the larger the SL thickness and polarization electric fields. The former can be attributed to the longer bond length of In−N than Ga−N. The latter can be ascribed to the lattice mismatch between the $Ga_{1-y}Mg_yN$ and $In_xGa_{1-x}N$ which leads to strain-induced piezoelectric polarization. The same is true for $Al_xGa_{1-x}N/GaN(0001)$ interfaces reported by Zhao et al.[57] Besides, under the same In and Mg compositions, the polarization electric fields in polar SLs are apparently stronger than those of semipolar ones. This is because the spontaneous polarized field caused by the noncoincidence of positive and negative charge centers is stronger in polar SLs. Semipolar sidewall QWs, lower In composition, and thinner QWs, these unique characteristics of the V-shaped pits reduce its polarization electric field, leading to smaller band bending at the interfaces of semipolar SLs. These findings are very consistent with the above band alignment results, which show that holes from the $Ga_{1-y}Mg_yN$ layer are easier to inject into

https://doi.org/10.1021/acsomega.3c09221
ACS Omega 2024, 9, 7163−7172

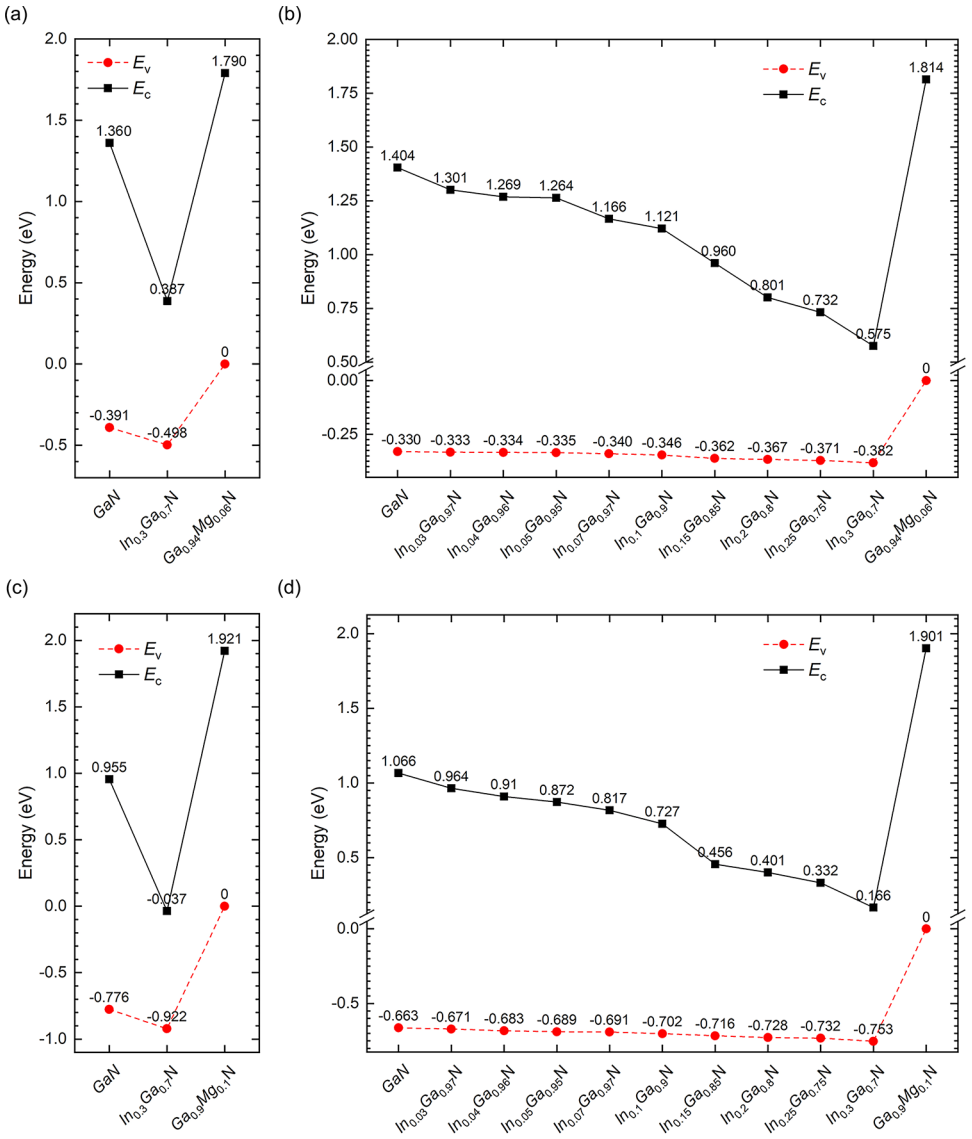

Figure 4. Conduction and valence band edges of (a) $In_xGa_{1-x}N$ (0001) and (b) $In_xGa_{1-x}N$ $(10\bar{1}1)$ relative to the band edges of $Ga_{0.94}Mg_{0.06}N$. Conduction and valence band edges of (c) $In_xGa_{1-x}N$ (0001) and (d) $In_xGa_{1-x}N$ $(10\bar{1}1)$ relative to the band edges of $Ga_{0.9}Mg_{0.1}N$.

the flat QWs via the sidewall of the V-shaped pits rather than the *c*-plane QWs.

Additionally, we conduct site-decomposed DOS calculations as well to understand the electron aggregations. Clearly, in all configurations shown in Figure 6, the obvious peaks near the Fermi level indicate that the 2p states of N are more inclined to bond with the 2p states of Mg than with Ga. The above-mentioned peaks also mean that there is strong hybridization between the N 2p orbital and the Mg 2p orbital, which is consistent with the calculation results of Li et al.[58] for $Al_{0.5}Ga_{0.5}N$:Mg/GaN SL. The DOS distribution is affected by the bonding of Mg and N atoms, which directly shift the valence band edges of all SLs toward higher energy. Moreover, as shown in Figure 5, the above shift tends to be larger as the Mg doping composition increases, resulting in a larger VBO. Meanwhile, this phenomenon explains well how the strong hybridization between the N 2p orbital and Mg 2p orbital results in higher energy of valence band edges in the $Ga_{1-y}Mg_yN$ layer than in the $In_xGa_{1-x}N$ layer. Therefore, the VBO of $In_xGa_{1-x}N/Ga_{1-y}Mg_yN$ is positive, both in semipolar and polar SLs, as displayed in Figure 4.

The energy-band diagram is used to discuss the role of V-shaped pits in carrier transport. Figure 7 depicts a schematic energy diagram of the carrier recombination process around a TD with small or large V-shaped pits. In the InGaN/GaN MQWs, carriers tend to diffuse laterally until they recombine.[59,60] There are several possible cases of the lateral diffusion of carriers. First, these carriers can recombine radiatively in the flat QWs. Second, in Figure 7c, it is found that they are likely to be captured by NR centers like TDs without V-shaped pits.[61] Third, near a TD with a small V-shaped pit, carriers are likely to be captured by TDs and eventually recombine nonradiatively. If the carriers diffuse to the vicinity of the TD with a larger V-shaped pit, the lateral diffusion of carriers to the TD can be greatly suppressed, thereby reducing the NR rate, which is in sharp contrast to the small V-shaped pits. The lower In composition in the sidewall QWs leads to a wider energy gap, which means that the valence band of sidewall QWs is in lower energy. There is an energy barrier for holes from the higher-energy flat QWs to diffuse laterally to the lower-energy sidewall QWs, which is the screening effect of V-shaped pits. Besides, Kim et al. found that

https://doi.org/10.1021/acsomega.3c09221
ACS Omega 2024, 9, 7163−7172

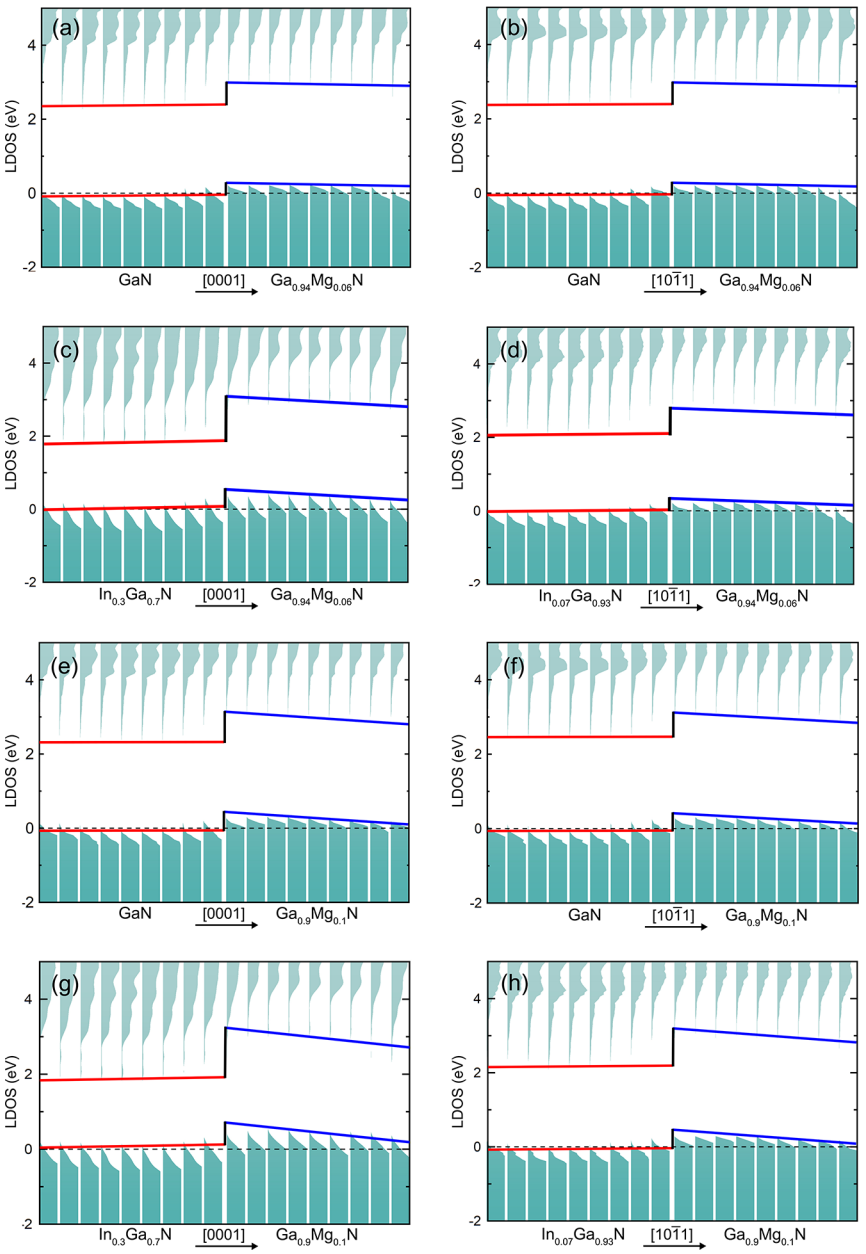

Figure 5. Layer-projected densities of states for (a) GaN/$Ga_{0.94}Mg_{0.06}N$ (0001), (b) GaN/$Ga_{0.94}Mg_{0.06}N(10\bar{1}1)$, (c) $In_{0.3}Ga_{0.7}N$/$Ga_{0.94}Mg_{0.06}N$ (0001), (d) $In_{0.07}Ga_{0.93}N$/$Ga_{0.94}Mg_{0.06}N$ ($10\bar{1}1$), (e) GaN/$Ga_{0.9}Mg_{0.1}N$ (0001), (f) GaN/$Ga_{0.9}Mg_{0.1}N$ ($10\bar{1}1$), (g) $In_{0.3}Ga_{0.7}N$/$Ga_{0.9}Mg_{0.1}N$ (0001), and (h) $In_{0.07}Ga_{0.93}N$/$Ga_{0.9}Mg_{0.1}N$ ($10\bar{1}1$). The Fermi level is set to 0 eV and denoted with black dashed lines.

Table 3. Calculated SL Thickness (Å) and Polarization Electric Field *E* (MV/cm) of Polar and Semipolar SLs with Different In and Mg Compositions[a]

direction	[0001]		[10$\bar{1}$1]									
In composition (%)	0	30	0	3	4	5	7	10	15	20	25	30
*p*1_*l*	47.30	48.42	44.27	44.55	44.61	44.74	44.73	45.13	45.57	46.00	46.35	46.82
$\lvert p1\_E_{In_xGa_{1-x}N}\rvert$	0.46	0.98	0.38	0.46	0.51	0.53	0.56	0.60	0.65	0.68	0.70	0.78
$\lvert p1-E_{GaMgN}\rvert$	0.96	1.36	0.45	0.66	0.74	0.82	0.86	1.00	1.05	1.11	1.21	1.34
*p*2_*l*	47.16	48.50	44.27	44.62	44.68	44.73	44.82	44.91	45.12	45.35	45.54	45.75
$\lvert p2\_E_{In_xGa_{1-x}N}\rvert$	0.13	1.36	0.03	0.09	0.11	0.18	0.26	0.30	0.54	0.78	0.92	1.14
$\lvert p2\_E_{GaMgN}\rvert$	2.89	3.22	2.84	2.88	2.94	3.01	3.03	3.06	3.16	3.20	3.31	3.32

[a]The lower Mg composition is denoted as P1, and the higher is denoted as P2.

the V-shaped pits of different sizes provide different energy barriers.[22] This can be explained by the fact that the valence band of smaller V-shaped pits is higher in energy than the larger one, as shown in Figure 7c. Therefore, in the process of

https://doi.org/10.1021/acsomega.3c09221
ACS Omega 2024, 9, 7163−7172

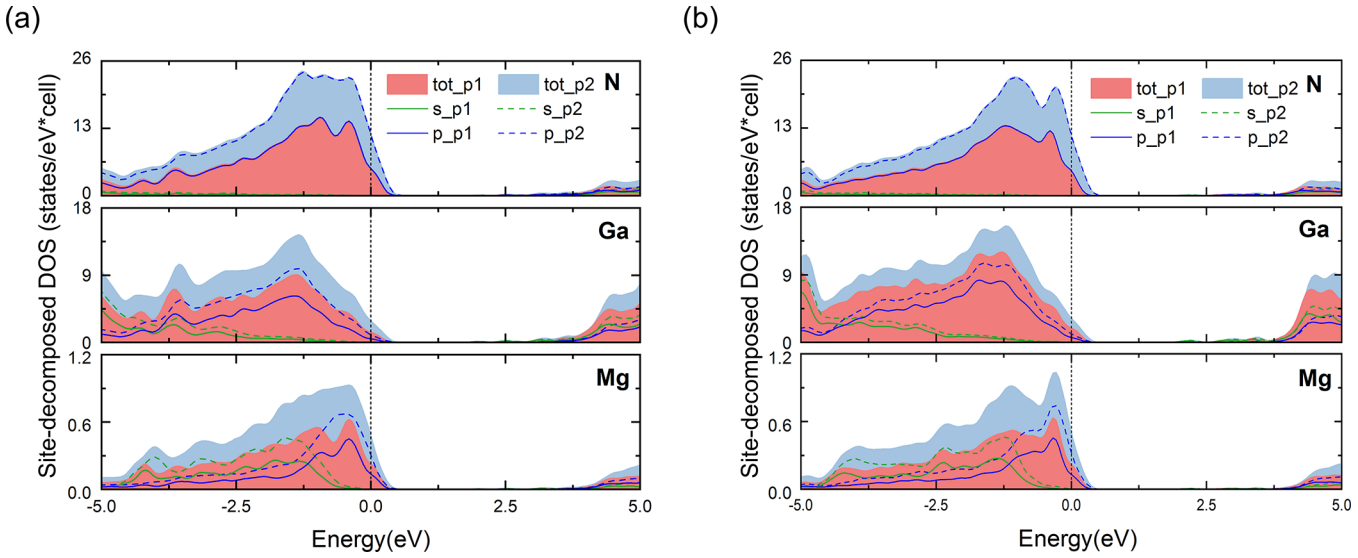

Figure 6. Site-decomposed DOS of (a) $In_{0.3}Ga_{0.7}N/Ga_{1-y}Mg_yN$ (0001) and (b) $In_{0.07}Ga_{0.93}N/Ga_{1-y}Mg_yN$ $(10\bar{1}1)$ (y = 0.06,0.1). The N/Ga atoms here are the nearest atoms around the Mg atoms. The Fermi level is set to 0 eV and is denoted with black dashed lines.

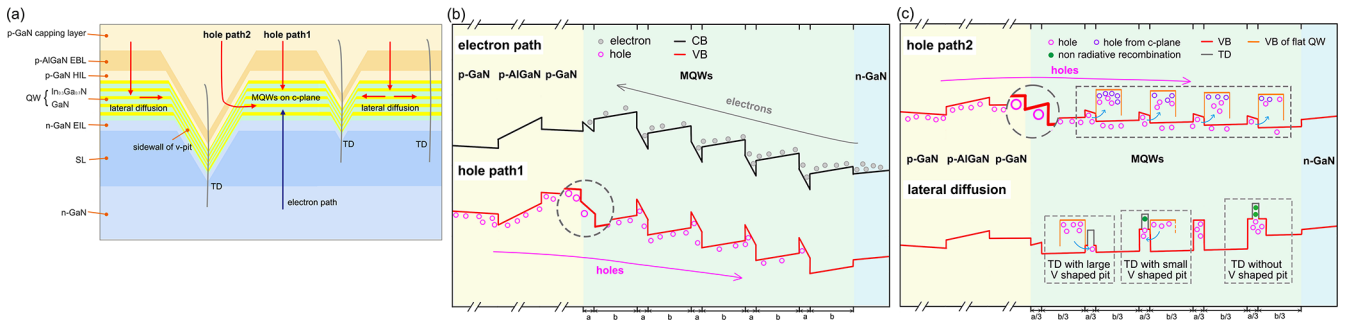

Figure 7. (a) Schematic diagram of the epitaxial structure of an InGaN-based LED embedded with large or small V-shaped pits. Energy-band diagram of (b) electron path and hole path 1 and (c) hole path 2 and lateral diffusion in (a). The quantum well thickness of flat QWs (sidewall QWs) is a (a/3) nm, and the quantum barrier thickness of flat QWs (sidewall QWs) is b (b/3) nm.

lateral diffusion of holes to TDs, smaller pits can only provide a lower energy barrier to prevent the holes. When the excitation energy reaches a certain value, holes can be easily captured by TDs, as depicted in Figure 7c.

Apart from screening dislocations, the V-shaped pits serve as a new path for holes to inject into the flat QWs as well. It is a common difficulty that the hole density distribution in different QWs is nonuniform. Due to the low mobility of holes, most of them are located in the top QW and are difficult to inject downward into the QWs below. Additionally, as depicted in Figure 7b, due to the strong polarization electric fields, which will lead to the quantum confined Stark effect (QCSE),[62−64] electrons and holes are separated spatially, which is detrimental to the luminous efficiency. However, the presence of V-shaped pits can effectively alleviate these two tough problems. Li et al. investigated the effect of InGaN MQWs embedded with V-shaped pits on carrier transport through 3D numerical modeling.[34] They found that when the hole current density is 1 A/cm^2, the hole is mainly distributed in the top and the third QW because of the top injection and sidewall injection. This means that the V-shaped pits are another way for holes to be injected into the flat QWs. While the hole current density increases to 20 A/cm^2, the hole concentration in the third and the fourth QW increases obviously. Holes need less excitation, i.e., a smaller energy barrier, to inject into the flat QWs via the sidewall QWs; therefore, the hole concentration in the third and fourth QW increases evidently. This indicates that V-shaped pits can alleviate the problem of severe carrier spatial separation, help the hole concentration distribution in the flat QWs be more uniform, and ultimately improve the emission efficiency, as shown in Figure 7c.

Although larger V-shaped pits can provide a higher energy barrier to suppress NR and promote the uniformity of hole density distribution to a large extent in flat QWs, the excessive size will bring about negative effects, as well. Such as poor optical output of LEDs[5] or the positive effect of V-shaped pits on efficiency droop will decrease when the pit diameter exceeds 150 nm.[26] Consequently, both the density and size of the V-shaped pits need to be cautiously designed for MQWs with such pits embedded.

4. CONCLUSIONS

In summary, the formation of the V-shaped pits and electronic properties of interfaces between $Ga_{1-y}Mg_yN$ and the sidewall of the pits are investigated by employing first-principles calculations. The formation energies of V-shaped pits of three sizes indicate that they are inclined to form in the N-rich environment. Furthermore, the analysis of the relaxed configuration of the V-shaped pits shows good stability of

https://doi.org/10.1021/acsomega.3c09221
ACS Omega 2024, 9, 7163−7172

the $(10\bar{1}1)$ facet. To further explore the effect of V-shaped pits on hole injection, the band alignment of the interfaces is studied. The VBO in the $In_{0.3}Ga_{0.7}N/Ga_{0.94}Mg_{0.06}N$ (0001) is 0.498 eV, while that in the $In_{0.07}Ga_{0.93}N/Ga_{0.94}Mg_{0.06}N$ $(10\bar{1}1)$ is 0.340 eV. Meanwhile, these band alignment results of the interfaces disclose that the valence band edges are in higher energy in the $Ga_{1-y}Mg_yN$ layer than in the $In_xGa_{1-x}N$ layer. Besides, to understand the underlying reason for the band alignment results, the PDOS and polarization electric field calculations are performed. The PDOS results imply that the strong hybridization between the N 2p orbital and Mg 2p orbital makes a big difference in the upward shifts of the valence band edges in the SLs. These phenomena reveal that holes are easier to inject into the flat QWs via the sidewall of V-shaped pits rather than the *c*-plane QWs and provide a theoretical basis for the growth of InGaN MQWs samples containing V-shaped pits.

AUTHOR INFORMATION

Corresponding Author

Zhihua Xiong − *Key Laboratory for Optoelectronics and Communication of Jiangxi Province, Jiangxi Science and Technology Normal University, Nanchang 330038, China;* orcid.org/0000-0002-0632-903X; Email: xiong_zhihua@126.com

Authors

Qingqing Feng − *Key Laboratory for Optoelectronics and Communication of Jiangxi Province, Jiangxi Science and Technology Normal University, Nanchang 330038, China*

Li Liu − *Key Laboratory for Optoelectronics and Communication of Jiangxi Province, Jiangxi Science and Technology Normal University, Nanchang 330038, China;* orcid.org/0009-0005-7186-4142

Yu Zhang − *Key Laboratory for Optoelectronics and Communication of Jiangxi Province, Jiangxi Science and Technology Normal University, Nanchang 330038, China;* orcid.org/0000-0002-3409-1401

Xiaolu Zhu − *Key Laboratory for Optoelectronics and Communication of Jiangxi Province, Jiangxi Science and Technology Normal University, Nanchang 330038, China;* orcid.org/0000-0002-3413-6489

Hai Kuang − *Key Laboratory for Optoelectronics and Communication of Jiangxi Province, Jiangxi Science and Technology Normal University, Nanchang 330038, China*

Mingbin Zhou − *Key Laboratory for Optoelectronics and Communication of Jiangxi Province, Jiangxi Science and Technology Normal University, Nanchang 330038, China*

Juanli Zhao − *Key Laboratory for Optoelectronics and Communication of Jiangxi Province, Jiangxi Science and Technology Normal University, Nanchang 330038, China*

Ning Wu − *Beijing Institute of Nanoenergy and Nanosystems, Chinese Academy of Sciences, Beijing 100083, China; School of Nanoscience and Technology, University of Chinese Academy of Sciences, Beijing 100049, China*

Complete contact information is available at: https://pubs.acs.org/10.1021/acsomega.3c09221

Notes

The authors declare no competing financial interest.

ACKNOWLEDGMENTS

This work was supported by the National Natural Science Foundation of China (Grant Nos. 12364013, 12264017), the Central Government Guide Local Science and Technology Development Fund Project (Grant No. 2022ZDD03088), the Key Research and Development Program in Jiangxi Province (Grant Nos. 20232BBE50024, 20224BBC41002), the Key Program of Jiangxi Provincial Natural Science Foundation (No. 20224ACB202005), the Foundation of Jiangxi Educational Committee (No. GJJ211117), and the Scientific Innovation Team of Optoelectronic Information in Nanchang. This work was carried out at the National Supercomputer Center in Tianjin, and the calculations were performed on Tianhe new generation supercomputer. We also thank Dr. Chen Lanli for the help in the discussions.

REFERENCES

(1) Piprek, J. Origin of InGaN/GaN light-emitting diode efficiency improvements using tunnel-junction-cascaded active regions. *Appl. Phys. Lett.* **2014**, *104* (5), No. 051118, DOI: 10.1063/1.4864311.

(2) Du, K.; Xiong, Z.; Ao, L.; Chen, L. Tuning the electronic and optical properties of two-dimensional gallium nitride by chemical functionalization. *Vacuum* **2021**, *185*, No. 110008, DOI: 10.1016/j.vacuum.2020.110008.

(3) Li, S.; Yu, L.; Qi, C.; Du, K.; Qin, G.; Xiong, Z. Different Effects of Mg and Si Doping on the Thermal Transport of Gallium Nitride. *Front. Mater.* **2021**, *8*, 322.

(4) Wu, X.; Liu, J.; Xiong, C.; Zhang, J.; Quan, Z.; Mao, Q.; Jiang, F. The effect of silicon doping in the barrier on the electroluminescence of InGaN/GaN multiple quantum well light emitting diodes. *J. Appl. Phys.* **2013**, *114* (10), 103102 DOI: 10.1063/1.4820450.

(5) Quan, Z.; Wang, L.; Zheng, C.; Liu, J.; Jiang, F. Roles of V-shaped pits on the improvement of quantum efficiency in InGaN/GaN multiple quantum well light-emitting diodes. *J. Appl. Phys.* **2014**, *116* (18), 183107 DOI: 10.1063/1.4901828.

(6) Zhang, Y.; Zhu, X.; Ao, L.; Xiong, Z. Thermodynamic Origin of High Efficiency in Long-Wavelength InGaN-Based LEDs on Si Substrates. *J. Phys. Chem. C* **2023**, *127* (15), 7520−7527.

(7) Kim, I. H.; Park, H. S.; Park, Y. J.; Kim, T. Formation of V-shaped pits in InGaN/GaN multiquantum wells and bulk InGaN films. *Appl. Phys. Lett.* **1998**, *73* (12), 1634−1636.

(8) Wu, X. H.; Elsass, C. R.; Abare, A.; Mack, M.; Keller, S.; Petroff, P. M.; Denbaars, S. P.; Speck, J. S.; Rosner, S. J. Structural origin of V-defects and correlation with localized excitonic centers in InGaN/GaN multiple quantum wells. *Appl. Phys. Lett.* **1998**, *72* (6), 692−694.

(9) Mahanty, S.; Hao, H.; Sugahara, T. V-shaped defects in InGaN/GaN multiquantum wells. *Mater. Lett.* **1999**, *41* (2), 67−71.

(10) Northrup, J. E.; Romano, L. T.; Neugebauer, J. Surface energetics, pit formation, and chemical ordering in InGaN alloys. *Appl. Phys. Lett.* **1999**, *74* (16), 2319−2321.

(11) Duxbury, N.; Bangert, U.; Dawson, P.; Thrush, E. J.; Van, D S W.; Jacobs, K.; Moerman, I. Indium segregation in InGaN quantum-well structures. *Appl. Phys. Lett.* **2000**, *76* (12), 1600−1602.

(12) Loganathan, R.; Prabakaran, K.; Pradeep, S.; Surender, S.; Singh, S.; Baskar, K. Influence of TMIn flow rate on structural and optical quality of AlInGaN/GaN epilayers grown by MOCVD. *J. Alloys Compd.* **2016**, *656*, 640−646.

(13) Cao, X. A.; Teetsov, J. A.; Shahedipour-Sandvik, F.; Arthur, S. D. Microstructural origin of leakage current in GaN/InGaN light-emitting diodes. *J. Cryst. Growth* **2004**, *264* (1−3), 172−177.

(14) Jeon, S. R.; Lee, S. J.; Jung, S. H.; Lee, S. H.; Baek, J. H.; Jeong, H.; Cha, O. H.; Suh, E. K.; Jeong, M. S. Effect of V-shaped defects on structural and optical properties of AlGaN/InGaN multiple quantum wells. *Journal of Physics D Applied Physics* **2008**, *41* (13), No. 132006.

(15) Ekinci, H.; Kuryatkov, V. V.; Forgey, C.; Dabiran, A.; Jorgenson, R.; Nikishin, S. A. Properties of InGaN/GaN MQW

LEDs grown by MOCVD with and without hydrogen carrier gas. *Vacuum* **2018**, *148*, 168−172.
(16) Tsai, S.-C.; Li, M.-J.; Fang, C.-H.; Liu, C.-P. Efficiency enhancement of blue light emitting diodes by eliminating V-defects from InGaN/GaN multiple quantum well structures through GaN capping layer control. *Appl. Surf. Sci.* **2018**, *439*, 1127−1132.
(17) Yang, J.; Zhao, D. G.; Jiang, D. S.; Chen, P.; Zhu, J. J.; Liu, Z. S.; Liang, F.; Liu, S. T.; Xing, Y. Suppression the formation of V-pits in InGaN/GaN multi-quantum well growth and its effect on the performance of GaN based laser diodes. *J. Alloys Compd.* **2020**, *822*, No. 153571, DOI: 10.1016/j.jallcom.2019.153571.
(18) Hangleiter, A.; Hitzel, F.; Netzel, C.; Fuhrmann, D.; Rossow, U.; Ade, G.; Hinze, P. Suppression of nonradiative recombination by V-shaped pits in GaInN/GaN quantum wells produces a large increase in the light emission efficiency. *Phys. Rev. Lett.* **2005**, *95* (12), No. 127402, DOI: 10.1103/PhysRevLett.95.127402.
(19) Lester, S. D.; Ponce, F. A.; Craford, M. G.; Steigerwald, D. A. High dislocation densities in high efficiency GaN-based light-emitting diodes. *Appl. Phys. Lett.* **1995**, *66* (10), 1249−1251.
(20) Carsten, N.; Heiko, B.; Lars, H.; Daniel, F.; Uwe, R. Emission and recombination characteristics ofGa1−xInxN/GaNquantum well structures with nonradiative recombination suppression by V-shaped pits. *Phys. Rev. B* **2007**, *76*, No. 155322, DOI: 10.1103/PhysRevB.76.155322.
(21) Cho, Y. H.; Kim, J. Y.; Kim, J.; Shim, M. B.; Hwang, S.; Park, S. H.; Park, Y. S.; Kim, S. Quantum efficiency affected by localized carrier distribution near the V-defect in GaN based quantum well. *Appl. Phys. Lett.* **2013**, *103* (26), 261101.
(22) Kim, J.; Cho, Y.-H.; Ko, D.-S.; Li, X.-S.; Won, J.-Y.; Lee, E.; Park, S.-H.; Kim, J.-Y.; Kim, S. Influence of V-pits on the efficiency droop in InGaN/GaN quantum wells. *Opt. Express* **2014**, *22* (9), A857−A866.
(23) Sheen, M.-H.; Kim, S.-D.; Lee, J.-H.; Shim, J.-I.; Kim, Y.-W. V-pits as Barriers to Diffusion of Carriers in InGaN/GaN Quantum Wells. *J. Electron. Mater.* **2015**, *44* (11), 4134−4138.
(24) Kim, D.-H.; Park, Y. S.; Kang, D.; Kim, K.-K.; Seong, T.-Y.; Amano, H. Combined effects of V pits and chip size on the electrical and optical properties of green InGaN-based light-emitting diodes. *J. Alloys Compd.* **2019**, *796*, 146−152.
(25) Chang, C. Y.; Li, H.; Shih, Y. T.; Lu, T. C. Manipulation of nanoscale V-pits to optimize internal quantum efficiency of InGaN multiple quantum wells. *Appl. Phys. Lett.* **2015**, *106* (9), No. 091104.
(26) Narihito, O.; Hiroyuki, K.; Kohei, S.; Yoichi, Y.; Kazuyuki, T. Controlling potential barrier height by changing V-shaped pit size and the effect on optical and electrical properties for InGaN/GaN based light-emitting diodes. *J. Appl. Phys.* **2015**, *117* (2), 25708.
(27) Shengjun, Z.; Xingtong, L. Effect of V-pits embedded InGaN/GaN superlattices on optical and electrical properties of GaN-based green light-emitting diodes. *Phys. Status Solidi (a)* **2016**, *214*, No. 1600782, DOI: 10.1002/pssa.201600782.
(28) Sharma, N.; Thomas, P.; Tricker, D.; Humphreys, C. Chemical mapping and formation of V-defects in InGaN multiple quantum wells. *Appl. Phys. Lett.* **2000**, *77* (9), 1274−1276.
(29) Bruckbauer, J.; Edwards, P. R.; Wang, T.; Martin, R. W. High resolution cathodoluminescence hyperspectral imaging of surface features in InGaN/GaN multiple quantum well structures. *Appl. Phys. Lett.* **2011**, *98* (14), 141908 DOI: 10.1063/1.3575573.
(30) Jahn, U.; Brandt, O.; Luna, E.; Sun, X.; Wang, H.; Jiang, D. S.; Bian, L. F.; Yang, H. Carrier capture by threading dislocations in (In,Ga)N/GaN heteroepitaxial layers. *Phys. Rev. B* **2010**, *81* (12), No. 125314, DOI: 10.1103/PhysRevB.81.125314.
(31) Li, Y.; Yun, F.; Su, X.; Liu, S.; Ding, W.; Hou, X. Deep hole injection assisted by large V-shape pits in InGaN/GaN multiple-quantum-wells blue light-emitting diodes. *J. Appl. Phys.* **2014**, *116* (12), 123101 DOI: 10.1063/1.4896362.
(32) Wu, X.; Liu, J.; Quan, Z.; Xiong, C.; Zheng, C.; Zhang, J.; Mao, Q.; Jiang, F. Electroluminescence from the sidewall quantum wells in the V-shaped pits of InGaN light emitting diodes. *Appl. Phys. Lett.* **2014**, *104* (22), 221101 DOI: 10.1063/1.4880731.
(33) Wu, X.; Liu, J.; Jiang, F. Hole injection from the sidewall of V-shaped pits into c-plane multiple quantum wells in InGaN light emitting diodes. *J. Appl. Phys.* **2015**, *118* (16), 164504 DOI: 10.1063/1.4934503.
(34) Li, C.-K.; Wu, C.-K.; Hsu, C.-C.; Lu, L.-S.; Li, H.; Lu, T.-C.; Wu, Y.-R. 3D numerical modeling of the carrier transport and radiative efficiency for InGaN/GaN light emitting diodes with V-shaped pits. *AIP Adv.* **2016**, *6* (5), No. 055208, DOI: 10.1063/1.4950771.
(35) Hikosaka, T.; Narita, T.; Honda, Y.; Yamaguchi, M.; Sawaki, N. Optical and electrical properties of (1−101)GaN grown on a 7 degrees off-axis (001)Si substrate. *Appl. Phys. Lett.* **2004**, *84* (23), 4717−4719.
(36) Shiojiri, M.; Chuo, C. C.; Hsu, J. T.; Yang, J. R.; Saijo, H. Structure and formation mechanism of V defects in multiple InGaN/GaN quantum well layers. *J. Appl. Phys.* **2006**, *99* (7), No. 073505, DOI: 10.1063/1.2180532.
(37) Tanikawa, T.; Hikosaka, T.; Honda, Y.; Yamaguchi, M.; Sawaki, N. Growth of semi-polar (11−22)GaN on a (113)Si substrate by selective MOVPE[C]. In *34th International Symposium on Compound Semiconductors*, 2007; p 2966.
(38) Wunderer, T.; Feneberg, M.; Lipski, F.; Wang, J.; Leute, R a R; Schwaiger, S.; Thonke, K.; Chuvilin, A.; Kaiser, U.; Metzner, S.; Bertram, F.; Christen, J.; Beirne, G. J.; Jetter, M.; Michler, P.; Schade, L.; Vierheilig, C.; Schwarz, U. T.; Draeger, A. D.; Hangleiter, A.; Scholz, F. Three-dimensional GaN for semipolar light emitters. *Physica Status Solidi B-Basic Solid State Physics* **2011**, *248* (3), 549−560.
(39) Kresse, G.; Furthmüller, J. Efficient iterative schemes for ab initio total-energy calculations using a plane-wave basis set. *Phys. Rev. B* **1996**, *54*, 11169.
(40) John, P.; Perdew, K.; Burke, M.; Ernzerhof, E. Generalized Gradient Approximation Made Simple. *Phys. Rev. Lett.* **1996**, *77*, 3865 DOI: 10.1103/PhysRevLett.77.3865.
(41) Monkhorst, H. J.; Pack, J. D. Special points for Brillouin-zone integrations. *Physical review. B, Condensed matter* **1976**, *13* (12), 5188−5192.
(42) Zhang, S. B.; Wei, S. H. Nitrogen solubility and induced defect complexes in epitaxial GaAs:N. *Physical review letters* **2001**, *86* (9), 1789−1792.
(43) Van De Walle, C. G.; Neugebauer, J. First-principles calculations for defects and impurities: Applications to III-nitrides. *J. Appl. Phys.* **2004**, *95* (8), 3851−3879.
(44) Zoroddu, A.; Bernardini, F.; Ruggerone, P.; Fiorentini, V. First-principles prediction of structure, energetics, formation enthalpy, elastic constants, polarization, and piezoelectric constants of AlN, GaN, and InN: comparison of local and gradient-corrected density-functional theory. *Phys. Rev. B* **2001**, *64* (4), 45208.
(45) Qin, Z.; Xiong, Z.; Qin, G.; Wan, Q. Behavior of aluminum adsorption and incorporation at GaN(0001) surface: First-principles study. *J. Appl. Phys.* **2013**, *114* (19), 113403.
(46) Lyons, J. L.; Janotti, A.; Van De Walle, C. G. Effects of carbon on the electrical and optical properties of InN, GaN, and AlN. *Phys. Rev. B* **2014**, *89* (3), No. 035204, DOI: 10.1103/PhysRevB.89.035204.
(47) Van De Walle, C. G.; Martin. Theoretical study of band offsets at semiconductor interfaces. *Physical review. B, Condensed matter* **1987**, *35* (15), 8154−8165.
(48) Janotti, A.; Van De Walle, C. G. Absolute deformation potentials and band alignment of wurtzite ZnO, MgO, and CdO. *Phys. Rev. B* **2007**, *75* (12), No. 12120, DOI: 10.1103/PhysRevB.75.121201.
(49) Jenn-Kai, T.; Ikai, L.; Keng-Lin, C.; Li-Wei, T.; Ji-Hao, H. Effect of N to Ga flux ratio on the GaN surface morphologies grown at high temperature by plasma-assisted molecular-beam epitaxy. *J. Appl. Phys.* **2004**, *95* (2), 460−460.
(50) Lee, W.; Lee, H. J.; Park, S. H.; Watanabe, K.; Kumagai, K.; Yao, T.; Chang, J. H.; Sekiguchi, T. Cross sectional CL study of the

https://doi.org/10.1021/acsomega.3c09221
ACS Omega 2024, 9, 7163−7172

growth and annihilation of pit type defects in HVPE grown (0001) thick GaN. *J. Cryst. Growth* **2012**, *351* (1), 83−87.
(51) Yu, Q. H. The Impact of V/III Ratio on GaN Growth by HVPE. *Adv. Mater. Res.* **2013**, *834*−*836*, 221−224.
(52) Li, C.; Zhang, K.; Zeng, Q.; Yin, X.; Chen, Z. High quality N-polar GaN films grown with varied V/III ratios by metal−organic vapor phase epitaxy. *RSC Adv.* **2020**, *10* (70), 43187−43192.
(53) Hangleiter, A.; Lahmann, S.; Netzel, C.; Rossow, U.; Kent, P. R. C.; Zunger, A. Electron and Hole Confinement in GaInN/GaN and AlGaN/GaN Quantum Wells. *MRS Online Proc. Lib. (OPL)* **2001**, *693*, 63.
(54) Hilmi, Ü; Asen, A. Band offsets in III-nitride heterostructures. *J. Phys. D: Appl. Phys.* **2002**, *35* (7), 591.
(55) Makimoto, T.; Kumarkura, K.; Nishida, T.; Kobayashi, N. Valence-band discontinuities between InGaN and GaN evaluated by capacitance-voltage characteristics of p-InGaN/n-GaN diodes. *J. Electron. Mater.* **2002**, *31* (4), 313−315.
(56) Dong, L.; Mantese, J. V.; Avrutin, V.; Oezguer, U.; Morkoc, H.; Alpay, S. P. Strain induced variations in band offsets and built-in electric fields in InGaN/GaN multiple quantum wells. *J. Appl. Phys.* **2013**, *114* (4), No. 043715, DOI: 10.1063/1.4816254.
(57) Zhao, J.; Xiong, Z.; Wu, N. Insight into the physical mechanism of AlxGa1xN electron blocking layer in GaN-based light emitting diodes. *AIP Adv.* **2018**, *8*, 105303 DOI: 10.1063/1.5046131.
(58) Li, J.; Kang, J. Band engineering in Al0.5Ga0.5N/GaN superlattice by modulating Mg dopant. *Appl. Phys. Lett.* **2007**, *91* (15), 152106.
(59) Danhof, J.; Schwarz, U. T.; Kaneta, A.; Kawakami, Y. Time-of-flight measurements of charge carrier diffusion in InxGa1-xN/GaN quantum wells. *Phys. Rev. B* **2011**, *84* (3), No. 035324, DOI: 10.1103/PhysRevB.84.035324.
(60) Danhof, J.; Solowan, H. M.; Schwarz, U. T.; Kaneta, A.; Kawakami, Y.; Schiavon, D.; Meyer, T.; Peter, M. Lateral charge carrier diffusion in InGaN quantum wells. *Physica Status Solidi B-Basic Solid State Physics* **2012**, *249* (3), 480−484.
(61) Fuhrmann, D.; Retzlaff, T.; Greve, M.; Hoffmann, L.; Bremers, H.; Rossow, U.; Hangleiter, A.; Hinze, P.; Ade, G. Dislocation screening and strongly increased internal quantum efficiency in heteroepitaxial GaN/AlxGa1-xN ultraviolet-emitting quantum wells. *Phys. Rev. B* **2009**, *79* (7), No. 073303, DOI: 10.1103/PhysRevB.79.073303.
(62) Zhao, D. G.; Jiang, D. S.; Zhu, J. J.; Wang, H.; Liu, Z. S.; Zhang, S. M.; Wang, Y. T.; Jia, Q. J.; Yang, H. An experimental study about the influence of well thickness on the electroluminescence of InGaN/GaN multiple quantum wells. *J. Alloys Compd.* **2010**, *489* (2), 461−464.
(63) Prabakaran, K.; Jayasakthi, M.; Surender, S.; Pradeep, S.; Sanjay, S.; Ramesh, R.; Balaji, M.; Gautier, N.; Baskar, K. Structural, morphological, optical and electrical characterization of InGaN/GaN MQW structures for optoelectronic applications. *Appl. Surf. Sci.* **2019**, *476*, 993−999.
(64) Romanowski, Z.; Kempisty, P.; Sakowski, K.; Strak, P.; Krukowski, S. Density Functional Theory (DFT) Simulations and Polarization Analysis of the Electric Field in InN/GaN Multiple Quantum Wells (MQWs). *J. Phys. Chem. C* **2010**, *114* (34), 14410−14416.

https://doi.org/10.1021/acsomega.3c09221
ACS Omega 2024, 9, 7163−7172